Applied Catalysis B: Environmental 330 (2023) 122457

Contents lists available at ScienceDirect

Applied Catalysis B: Environmental

journal homepage: www.elsevier.com/locate/apcatb

Porous carbon supported Lewis acid-base sites as metal-free catalysts for the carbonylation of glycerol with urea

He Wang [a,1], Yunzuo Cui [b,1], Jinghui Shi [b,*], Xin Tao [a,*], Guangshan Zhu [a]

[a] Key Laboratory of Polyoxometalate and Reticular Material Chemistry of Ministry of Education, Faculty of Chemistry, Northeast Normal University, 5268 Renmin Street, Changchun 130024, PR China
[b] Key Laboratory of Preparation and Applications of Environmentally Friendly Materials, Jilin Normal University, Ministry of Education, Changchun 130103, PR China

ARTICLE INFO

Keywords:
Lewis acid-base sites
Porous carbon
Metal-free catalysis
Glycerol carbonate
React-IR

ABSTRACT

Glycerol carbonylation is one of the most efficient reaction pathways to utilize glycerol, one of the by-products in biodiesel industry. So far, the vast majority of the reported glycerol carbonylation catalysts contain metals, which are not environmentally friendly. The recent emerging Lewis acid-base chemistry had provided powerful alternatives for metal-free catalysis. Here, we report the facile preparation of the B,N,P co-doped porous carbon materials, and the Lewis acidic/basic defects were detected in their structures. The obtained material BNP@C-800 exhibits excellent catalytic performance for the catalytic carbonylation of glycerol with urea, which achieved up to 93.6% glycerol conversion and 93.7% glycerol carbonate selectivity under metal-free conditions. The catalyst BNP@C-800 could be easily recycled for five times only by simple treatments without obvious loss in catalytic activity. In addition, the key reaction intermediate glycerol urethane was successfully characterized via React-IR spectroscopy. Furthermore, a heterogeneous Lewis acid-base synergistic catalysis mechanism is proposed.

1. Introduction

The increasing market demand of biodiesel has resulted in the excess of glycerol as a by-product in its production process, which brought new problems and challenges to the sustainable development of biodiesel. Excess glycerol is not only difficult to reprocess, but also increases the cost of the biodiesel industry. Therefore, on the basis of the biodiesel production process, it is an urgent problem to seek a method with higher economic benefits to effectively utilize glycerol [1,2]. Glycerol could derivate thousands of downstream high value-added products through reactions such as dehydration, hydrogenation, oxidation, esterification and microbial degradation, such as diol, propenol, acrolein, acrylic acid, glyceric acid etc [3–6]. Among these synthetic strategies, the synthesis of glycerol carbonate (GC) by glycerol carbonylation is one of the most efficient glycerol reaction pathways.

As a special biochemical, GC has the characteristics of high boiling point, low volatility, strong polarity and low-toxicity. It is widely used in food, medicine, cosmetics, textiles, coatings, plastics, machinery, military, aviation, aerospace, integrated circuits and new energy and other fields [7,8]. GC has great potential in many application fields, such as reactive protic solvents, surfactants and pharmaceuticals. More importantly, GC can also serve as an important building block for the preparation of polymers such as polycarbonates, polyglycerol esters, hyperbranched polyols and non-isocyanate polyurethanes [9,10]. The synthetic methods of GC include phosgene method, CO oxidative carbonylation method, transesterification method, glycerol carbonylation method and CO_2 conversion method [11–15]. Among them, the glycerol carbonylation with urea as raw materials is considered to be an efficient molecular reaction process, which is inexpensive and thermodynamically favorable. In addition, it avoids the formation of azeotropic system and facilitates product separation. The by-product ammonia gas produced in the carbonylation process could also be used as the raw material for synthesizing urea [16,17]. Therefore, more and more researchers have paid more attention to this research field. In earlier studies, Lewis acids $ZnCl_2$, ZnO, ZnI_2, ZnF_2, $ZnBr_2$ were used as homogeneous catalysts to activate urea and glycerol at molecular level [18]. High yield and selectivity of glycerol carbonate can be obtained by regulating the catalyst structures. However, the poor stability and recyclability of catalysts are major problems facing the scientific and industrial circles. In recent years, heterogeneous catalysts, such as

* Corresponding authors.
E-mail addresses: shijinghui0404@163.com (J. Shi), taox091@nenu.edu.cn (X. Tao).
[1] The two authors contribute equally to the work.

https://doi.org/10.1016/j.apcatb.2023.122457
Received 17 September 2022; Received in revised form 31 January 2023; Accepted 8 February 2023
Available online 10 February 2023

hydrotalcite-based catalysts (HT(Mg/Zn/Al)) [19], zeolite-based catalysts (Zn-FAU) [20], boiler waste ash-based catalysts (K_2SiO_3) [21], tungsten-based catalysts (WO_3-TiO_2) [22], imidazole-based catalysts (PS-$(Im)_2ZnBr_2$) [23], mesoporous crystalline materials (Zn/MCM-41) [24], functionalized network metal-organic frameworks (F-IRMOF-3 (BuI)) [25], [PS-$(Im)_2MX_2$] [26] and other catalysts (γ-zirconium phosphate [27], La_2O_3 [28], $La_2Cu_{0.5}Fe_{0.5}O_4$ [29], etc.) were found to be able to maintain their own structure during the catalytic reactions. The stable active sites in heterogeneous catalysts endow them with long life time, which is beneficial for their recyclability in the catalysis process. However, there are still problems such as complicated preparation and high cost have restricted their application in GC production. In addition, the vast majority of the reported GC production catalysts contain metals, which are not in line with the concept of green chemistry (Scheme 1). Therefore, it is an urgent task to synthesize metal-free catalysts with good catalytic performance by simple methods with low-cost raw materials.

The recently active Lewis acid-base chemistry has provided alternative tools for homogeneous catalysis under metal free conditions. Homogeneous Lewis acid-base synergistic catalysts are widely used in catalysis and synthetic chemistry and have received continuous attention in recent years [30,31]. However, the poor stability and recyclability of homogenous Lewis acid-base synergistic catalysts have seriously restricted their applications in large-scale catalytic reactions. Therefore, the stable solid state Lewis acid-base synergistic catalysts have attracted great interests for heterogeneous catalysis both in fundamental research and practical applications [32–35]. Meanwhile, porous carbon materials have already played important and diverse roles in solving global energy and environmental problems due to their high specific surface area, low density, good chemical stability and eco-friendly nature. Based on these considerations, it is our great interest to introduce the Lewis acid-base sites into porous carbon materials. We expect that the unique spatial confinement effect of porous carbon materials could stabilize the Lewis acid-base sites and maintain excellent catalytic performance for GC production.

Herein, we report the fabrication of porous boron/nitrogen/phosphorus codoped carbon materials (BNP@C) by sol-gel method. These materials are characterized by various physicochemical techniques and show typical characters of porous carbon and active Lewis acid-base sites. Notably, it is found that the resultant BNP@C materials serve as metal-free catalysts for carbonylation of glycerol with urea, which exhibits remarkably high catalytic activity and recyclability. The possible reaction mechanism is considered to follow a Lewis acid-base synergistic catalysis reaction pathway.

2. Experimental

2.1. Chemicals

Sucrose, boric acid, $Al(NO_3)_3{\cdot}9\ H_2O$, 85% H_3PO_4, melamine, acetic acid, nitric acid, glycerol, urea, boron nitride (BN) was commercially available and were used as received.

2.2. Catalysts preparation

2.2.1. Synthesis of BNP@C-T

Typically, sucrose (10.3 g) and boric acid (2.5 g) were added into 140 mL distilled water, and the resulting reaction mixture was stirred until all the solid materials were completely dissolved. Then Al $(NO_3)_3{\cdot}9\ H_2O$ (10.0 g) was added to the reaction mixture, which was the stirred until it was completely dissolved. Afterwards, H_3PO_4 (5.5 mL) and melamine (0.5 g) were added, and the resulting mixture was transferred to a 40 °C water bath. Then, an appropriate amount of acetic acid was added until the solution was completely clear. The resulting solution was dried over a water bath at 80 °C to give the prepolymer. Finally, the composite was pretreated at 300 °C in open air for 10 min, and then carbonized at certain temperature (700, 800 and 900 °C, respectively) for 6 h under an argon flow. The carbonized black

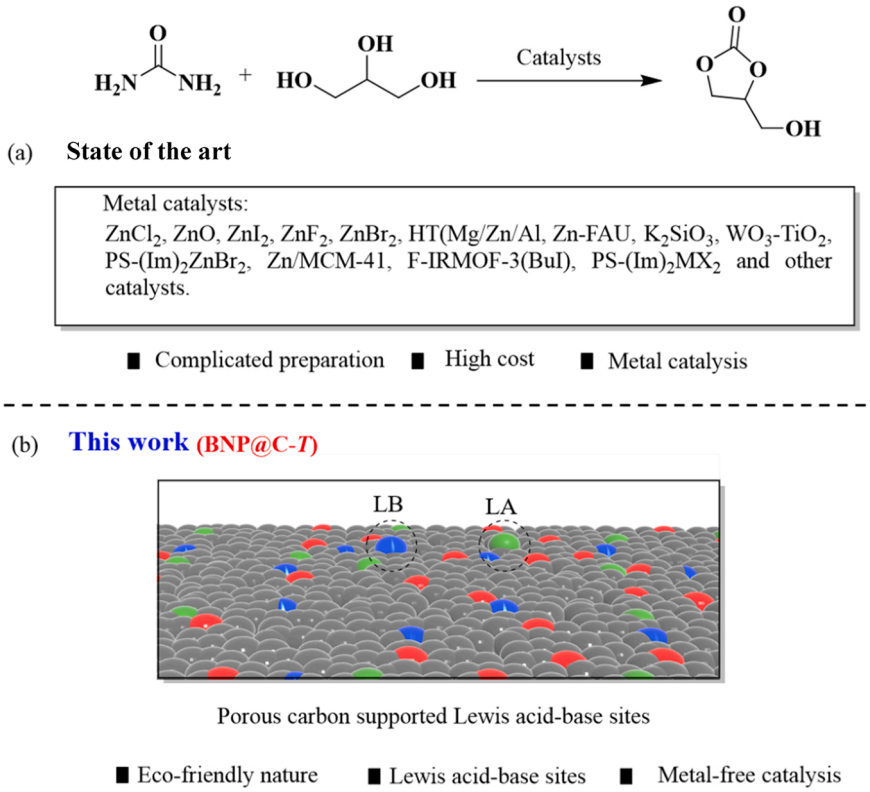

Scheme 1. Catalytic carbonylation of glycerol with urea.

composite was treated with 4 M HNO_3 solution at 60 °C, filtered and washed with deionized water. The resulting materials were finally obtained by vacuum drying at 100 °C. The synthesized B,N,P-doped carbon materials are denoted as BNP@C-*T*, where *T* stands for carbonized temperature, and the obtained carbon materials with different carbonized temperatures are denoted as BNP@C-700, BNP@C-800 and BNP@C-900, respectively.

2.2.2. Synthesis of BPO_4

BPO_4 was prepared according to the procedures described in reference [36]: H_3PO_4 (0.02 mol) and H_3BO_3 (0.02 mol) were dissolved in 30 mL deionized water. The obtained solution was placed on a water bath at 80 °C for 12 h. After it was completely dried, the residual solid was calcined at 600 °C for 2 h under air atmosphere and then washed with deionized water to neutral.

2.2.3. Synthesis of SC

Sucrose (10.3 g) was added to 140 mL distilled water. After it was completely dissolved, the solution was dried in a water bath at 80 °C to obtain the prepolymer. Then, the composite was pretreated for 10 min at 300 °C in open air and carbonized for 6 h at 800 °C under an argon flow, which was denoted as SC.

2.3. Characterization

Fourier transforminfrared (FT-IR) spectra of samples were obtained on a NICOLET iS50 spectrometer by the conventional KBr pellet technique. Raman spectra were collected on LabRAM HR Evol spectrometer using 488 nm excitation laser. Transmission electron microscopy (TEM) images and the high-angle annular dark field STEM (HAADF-STEM) images were taken with a TEM tian G2 60–300 with probe corrector. X-ray diffractometer (XRD) pattern was tested on a Rigaku Smart Lab X-ray diffractometer (40 kV, 30 mA) using Ni-filtered Cu Kα radiation. The N_2 adsorption-desorption isotherms were measured at 77.3 K, using a BELSORP-max II adsorption analyzer. Samples were degassed at 373 K for 12 h before measurements. The microstructure and surface morphology of the samples were obtained by Scanning Electron Microscope (SEM) of Hitachi S-4300. X-ray photoelectron spectroscopy (XPS) was performed on Thermo Scientific Escalab 250Xi with an Al-Kα X-ray source. The binding energies of elements were calibrated using the C 1 s photoelectron peak at 284.6 eV. ICP-AES (LEEMAN, American) was performed to analyze Al content.

The Lewis acidity-basicity properties of BNP@C-800 were determined through temperature-programmed desorption-mass spectrometry (TPD-MS). In a typical experiment, 100 mg of BNP@C-800 was treated at 800 °C for 2 h, and then cooled down to 50 °C in Ar. The sample was exposed to 10% CO_2/Ar or NH_3/Ar mixture flow for 1 h. Then the sample was flushed with Ar flow at 50 °C to remove the weakly adsorbed species from the sample. The TPD profile of the sample was then recorded by increasing the temperature from 50° to 800°C at a heating rate of 10 °C/min under 20 mL/min of Ar flow. The desorbed CO_2 and NH_3 were detected on-line by a quadrupole mass spectrometer (Hiden HPR-20). The mass signal at $m/z = 44$ and $m/z = 17$ were used to determine the amount of desorbed CO_2 and NH_3. The concentration of Brønsted acidic/basic groups on the surface of materials was determined by acid-base titration method with 0.05 M solution of HCl and NaOH.

React IR Experimental Details: For the React IR kinetic experiments, the reaction spectra were recorded using a React IR 15 with Liquid N_2 MCT Detector, Ag* 9.5 mm * 1.5 m Fiber probe Interface and DiComp (Diamond) probe Tip from Mettler-Toledo AutoChem. Data manipulation was carried out using the iC IR software, version 4.3.

2.4. Catalytic performance

In a typical experiment, glycerol (4.6 g, 0.05 mol) was added to a 100 mL two-neck round-bottomed flask and treated at 80 °C to reduce the viscosity, urea (4.5 g, 0.075 mol) of was added into the flask under stirring. And after the urea was dissolved, the catalyst (5% by mass of glycerol) was added to the flask. The reaction was carried out under vacuum (7.0 kPa) and the reaction temperature and sampling time were set according to the investigated conditions. A cooling trap (liquid nitrogen) was connected between the upper end of the reflux condenser and vacuum pump to recycle the NH_3 during the reaction. After completion of the reaction or stipulated time, it is necessary to turn off the vacuum pump and a certain amount of reaction mixture was filtered through a 0.45 μm syringe filter. The filtrate is diluted in N,N-Dimethylformamide and then tetraethylene glycol was added. The reaction products (0.2 μL) were quantitatively analyzed by a gas chromatography (Shimadzu, GC-2010 Plus) equipped with a Wondacap WAX capillary column (30 m) and FID detector. The glycerol conversion, GC selectivity, GC yield and by-product selectivity were calculated by the internal standard method (tetraethylene glycol) and the calculation method is described in the Supplementary Material. The reaction products were qualitatively analyzed by gas chromatography-mass spectrometer (ISQ-LT).

A typical cycle experiment for synthesizing glycerol carbonate: the catalyst is filtered out from the reaction solution, washed with ethanol several times and dried in vacuo. The recycled catalyst is used for a repeat catalysis experiment under the same reaction conditions.

3. Results and discussion

3.1. Preparation of BNP@C-T

In this work, a new type of carbon material was synthesized via sol-gel process using “organic molecular template method”, sucrose as a soft template [37] and simultaneously as a carbon source [38], melamine as a nitrogen source, H_3BO_3 as a boron source and H_3PO_4 as a phosphorus source (Fig. 1). In the preparation process, the sucrose molecule itself contains a plurality of hydroxyl groups and the hydroxyl groups can form an aggregate similar to surfactant micelles between molecules through hydrogen bonds. Sucrose, melamine and boric acid all interacted with $Al(NO)_3$ through hydrogen bonds to form an organic-inorganic mesophase, and one-pot synthesis of BPO_4 from H_3PO_4 and the excess H_3BO_3. After charing, $Al(NO)_3$ formed the mesoporous Al_2O_3, which is surrounded by carbon and on the carbon surface. Then, it is carbonized in an inert atmosphere at high temperature and all the structures are firmly linked together to form a carbon grid (XRD patterns shown in Fig. S1). After two heat-treatments, the mass loss is about 43 ~ 48%. Finally, the Al_2O_3 in the carbon material was washed away with diluted HNO_3 (4 M) to form a boron-nitrogen-phosphorus co-doped porous carbon material BNP@C-*T*.

3.2. Characterization of BNP@C-T

The obtained FTIR spectra of the BNP@C-*T* are also analyzed to reveal the structure of these materials. As can be seen from Fig. 2a, a broad peak near 3436 cm^{-1} can be assigned to the vibrational absorption of -OH. The aromatic C═C stretching vibration absorption appears at 1606 cm^{-1}, indicating the presence of a sp^2 hybridized honeycomb lattice [39]. The absorption peaks at 553 cm^{-1} and 630 cm^{-1} were assigned to the bending vibrations of O-P-O in PO_4 and O-B-O in BO_4, respectively. The broad signal at 1090 cm^{-1} was assigned to the asymmetric vibrations of P-O in PO_4. Additionally, the peak at 932 cm^{-1} was attributed to B-O stretching in BO_4. The peaks around 1383 cm^{-1} were attributed to the in-plane B-N stretching vibration [40–42].

The effects of carbonization temperatures on structure of BNP@C-*T* were investigated by using XRD as shown in the Fig. 2b. For these three materials, 24.5°, 40.0°, 48.8° and 63.7°, were respectively assigned to the (101), (112), (121) and (213) planes of cubic BPO_4 crystal phase (JCPDS 34–0132) confirming the existence of some grain crystalline of

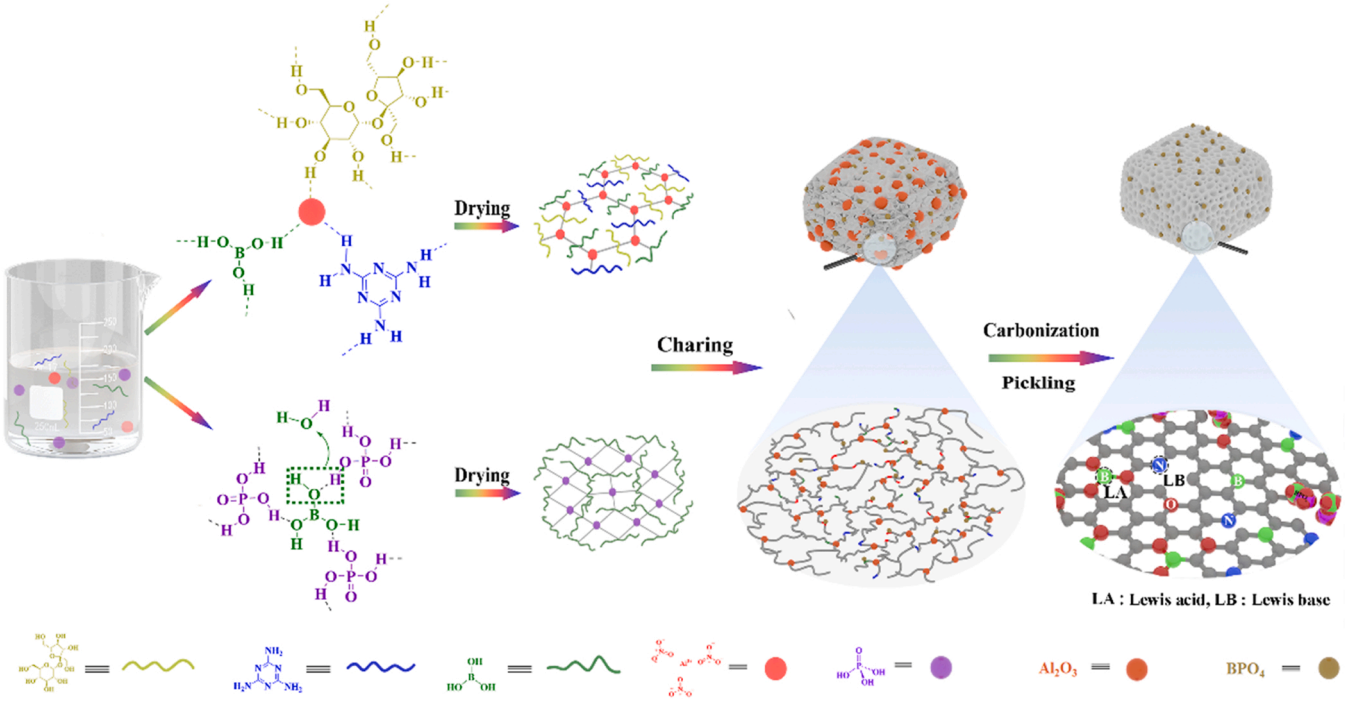

Fig. 1. Schematic presentation of the fabrication of BNP@C-*T*.

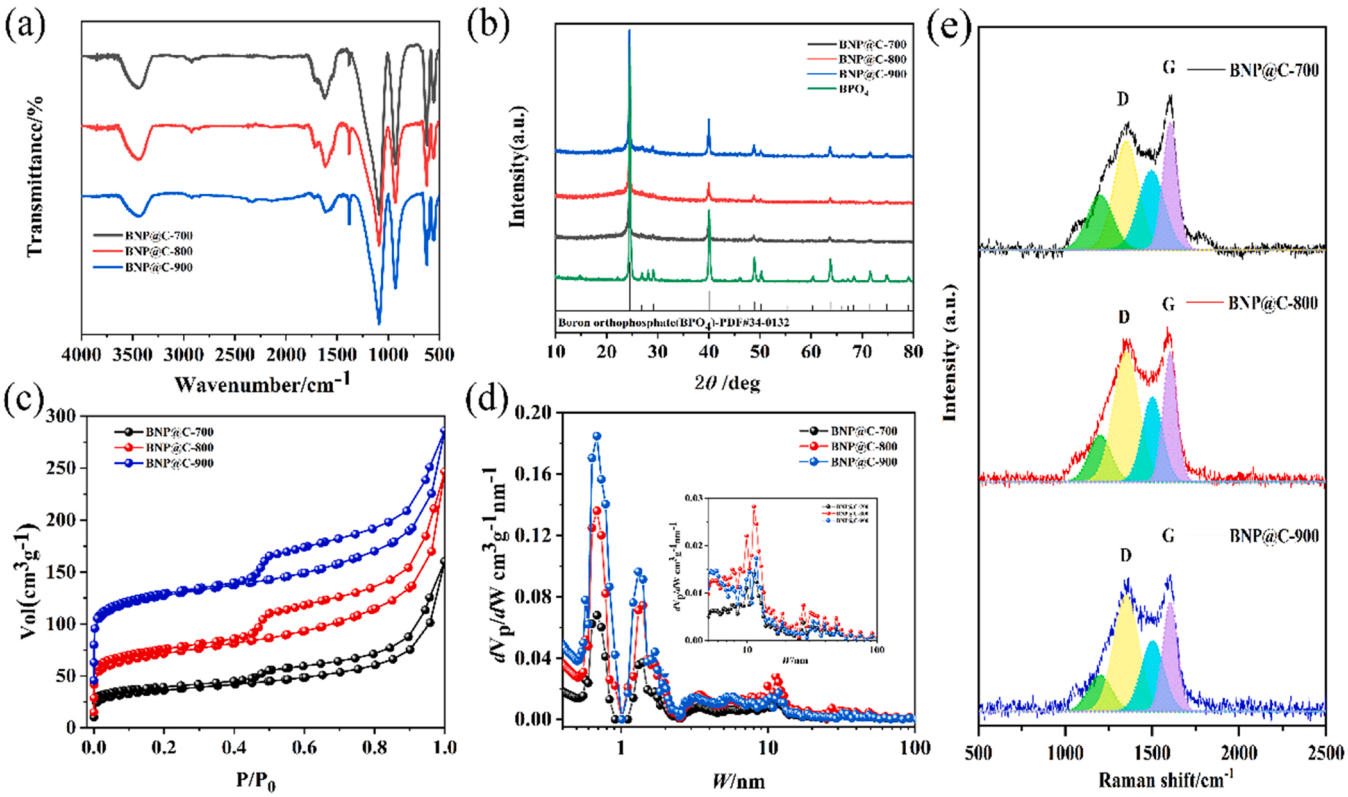

Fig. 2. (a) FTIR spectra, (b) XRD patterns, (c) Nitrogen adsorption/desorption isotherms, (d) pore size distributions (Pore size distribution that calculated using DFT method.) and (e) Raman spectra of BNP@C-*T* catalysts.

BPO_4 in these materials [42]. The crystallization becomes stronger with the increasing of carbonization temperature. It is worth mentioning that the amorphous graphite-like phase structure was not detected, which may be covered by the strong diffraction signal of BPO_4 from 700 °C to 900 °C. The XRD pattern of SC (Fig. S2) exhibits two broad peaks at 25° and 44°, which can be indexed to (002) and (101) diffractions for glass-like carbon, indicating the amorphous characteristic of the SC [43].

It can be seen from the nitrogen adsorption and desorption isotherm (in Fig. 2c) that the three carbon materials have similar nitrogen

adsorption and desorption curves. According to the latest IUPAC classification, the three carbon materials exhibit the type IV isotherm. The low-pressure region ($P/P_0 < 0.001$) has a higher nitrogen adsorption capacity, which proves that the material has rich microporous structure [44]. Furthermore, there is an obvious hysteresis and a slight rise in the medium- and high-pressure region, which is consistent with the H4 type hysteresis loop. This indicates the micro-mesoporous nature of these materials, which is also verified by the pore size distribution map (Fig. 2d). It is also found that the BET specific surface areas micropore volumes of these materials are dependent on their carbonization temperature. With the increase of the carbonization temperature, the specific surface areas and micropore volumes of the three carbon materials increases (Table 1), respectively. The micropore diameters of these materials are mainly around 0.7 nm and 1.3 nm.

The structure of the BNP@C-*T* were characterized by Raman spectra, as shown in the Fig. 2e. The characteristic D and G bands were located around 1353 and 1593 cm^{-1}, respectively. D-peak represents the defects of C atom crystal and G-peak represents the in-plane stretching vibration mode of the sp^2-hybridized C atoms. The I_D/I_G value is usually used to reflect the disorder degree of the carbon material, the higher the I_D/I_G value, the greater the number of defect sites in the carbon material. With the increase of carbonization temperature, the I_D/I_G value of BNP@C-*T* also increases: 1.14 (BNP@C-700) < 1.79 (BNP@C-800) < 1.81 (BNP@C-900). This indicates the introduction of oxygenated groups generated on the material's surface through chemical activation with HNO_3, which lead to surface disorders. Similar results were also reported in the literatures [45,46]. Due to the introduction of B and N elements into the material skeleton, more defect sites could be formed, which are considered as catalytically active Lewis acid-base sites for carbonylation of glycerol with urea [47].

The morphology and microstructure of BNP@C-800 was studied by SEM and TEM, and the images are shown in Fig. 3. SEM images (Fig. 3a) show that there are some honeycomb holes on the surface of BNP@C-800, which may be formed after the removal of Al_2O_3. Some polymer spheres can be seen in Fig. 3i, which could be inferred to be BPO_4 on basis of IR and XRD patterns. Fig. 3j-l show the microstructure of BPO_4 under the field emission transmission electron microscope. The well-resolved lattice fringes with spacing of 2.25 and 3.64 nm suggest (101) and (112) interplanar distance of BPO_4, which also proves the existence of BPO_4. The stack of BPO_4 spheres could also indirectly explain the slight rise of the medium-high pressure region in the nitrogen isothermal adsorption desorption curve. In addition, the distribution of elements in BNP@C-800 sample was demonstrated by HAADF-STEM and SEM mapping. As shown in Fig. 3b-h, C, O, N, B and P are well dispersed in BNP@C-800.

The surface functional groups of BNP@C-*T* were characterized by XPS measurements and the contents of main elements on the surface of the material were calculated. XPS test also showed that the BNP@C-*T* do not contain Al element (Fig. S3) on their surfaces. Inductively coupled plasma atomic emission analysis (ICP-AES) revealed that no detectable Al was observed. The BNP@C-*T* materials prepared with different carbonization temperature exhibit similar C 1 s, N 1 s, O 1 s, P 2p and B1s spectra, indicating that these materials have similar surface composition. The B 1 s, N 1 s, P 2p, spectra of BNP@C-*T* are shown in Fig. 4.

According to relevant literatures, the peak of C 1 s could be deconvoluted into three peaks [43,48]. The peak in the region of 284.7 eV usually corresponds to pure graphitic or amorphous C-C. The peak in the region of 286.1–286.2 eV could be assigned to sp^2-carbons such as C═N/C═O groups, carbon in phenolic, alcohol or ether. The peak around (288.2–288.3 eV) could be attributed to the sp^3carbon such as C-N/C-O bonding states, and carbons in carbonyl or quinone groups. (Fig. S4). The O 1 s peak can be integrated into three peaks [47,49], which could be assigned to oxygen in highly conjugated carbonyl (531.2 eV), in hydroxyl or ether (532.43 eV), and in anhydride, lactone, carboxylic acid or NO_x (533.33 eV), respectively (Fig. S5). Notably, the Lewis acidic boron species for instance BC_3 (189.8 eV), BCO_2 (192.9 eV), BO_3 (194.1 eV) and other two characteristic peaks, BN (191.0 eV) and BO_4 (191.4 eV) could be assigned in B 1 s spectra of BNP@C-*T* [50]. These groups would potentially serve as Lewis acid components in heterogenous Lewis acid-base synergistic catalysis. The Lewis basic nitrogen in pyridine-N (398.0–398.3 eV), pyrrole-N (399.5–399.8 eV), graphite-N (401.0 eV) and nitrogen oxide (405.0–405.2 eV) could be assigned in N 1 s spectra [47]. In P 2p spectra, a peak around 134.65 eV could be attributed to the phosphorous in the P-O bond [51]. These groups could potentially serve as Lewis base components in heterogenous Lewis acid-base synergistic catalysis. These results prove that B and N elements have been successfully doped into the carbon skeleton, and P element mainly exists in the BPO_4 species on the surface of carbon materials. As can be seen from Table 2, with the increase of carbonization temperature, the surface composition of BNP@C-700 and BNP@C-800 are slightly different. However, continuing increase of the carbonization temperature to 900 °C leads to the obvious loss of the surface composition in BNP@C-900.

TPD-MS analyses were applied to reveal the Lewis acidity and basicity of BNP@C-800 (Fig. 5). The NH_3-TPD-MS profile of BNP@C-800 can be deconvoluted into three peaks with desorption temperatures, respectively (Fig. 5a). The desorption peaks of NH_3 indicated that the BNP@C-800 has weakly acidic sites and medium-strongly acidic sites, which are mainly Lewis acids [52,53]. While, the CO_2-TPD-MS curve of BNP@C-800 has obvious desorption peaks at 80 ~ 500 ℃. The peaks at 80 ~ 150 ℃ and 350 ~ 500 ℃ suggest that BNP@C-800 has Lewis basic sites coming from pyridine N species [54,55]. Other peaks indicate that this material has other Lewis basic sites (e.g. pyrrole-N) on the surface. The NH_3/CO_2-TPD-MS curves of BNP@C-800 were also compared with a blank experiment (without pre-adsorption of CO_2 or NH_3) and significant differences were observed (Fig. S6), thus excluding the effect of the decomposition of surface groups on the BNP@C-800. All these characterization results have suggested that the coexistence of various Lewis acidic/basic sites on the surface of BNP@C-*T* materials, which may serve as potential catalysts for carbonylation of glycerol with urea.

Table 1
The textural parameters of BNP@C-*T* materials.

Sample	S_{BET}[a] (m^2g^{-1})	S_L[b] (m^2g^{-1})	PV[c] (cm^3g^{-1})	MPV[d] (cm^3g^{-1})
BNP@C-700	130	156	0.226	0.047
BNP@C-800	258	382	0.350	0.102
BNP@C-900	335	477	0.364	0.122

[a] Surface area calculated from nitrogen adsorption isotherms at 77.3 K using BET equation.
[b] Surface area calculated from nitrogen adsorption at 77.3 K using Langmuir equation.
[c] Pore volume calculated from nitrogen isotherm at $P/P_0 = 0.990$, 77.3 K.
[d] Micropore volume calculated from the nitrogen isotherm at $P/P_0 = 0.050$ [44].

3.3. Catalytic properties

It is well known that carbonylation of glycerol with urea is a very complex reaction process, and the products selectivity is closely related to the inherent properties of the catalyst and reaction conditions. The product distribution on the BNP@C catalytic systems was shown in Scheme 2, such as glycerol urethane (I), glycerol carbonate (GC) and (2-oxo-1,3-dioxolan-4-yl)methyl carbamate (II).

The catalytic performance of SC, ordered BPO_4, BN and BNP@C-800 catalysts for carbonylation of glycerol with urea under same conditions were investigated and the results are shown in Fig. 6a and Table S1. Among them, BN and BPO_4 as metal-free are active for the carbonylation of glycerol with urea, which is mainly attributed to the presence of Lewis acid-base sites on the surface of catalysts. However, the GC yields catalyzed by SC, BN and BPO_4 are all lower than 40.0%, which are not

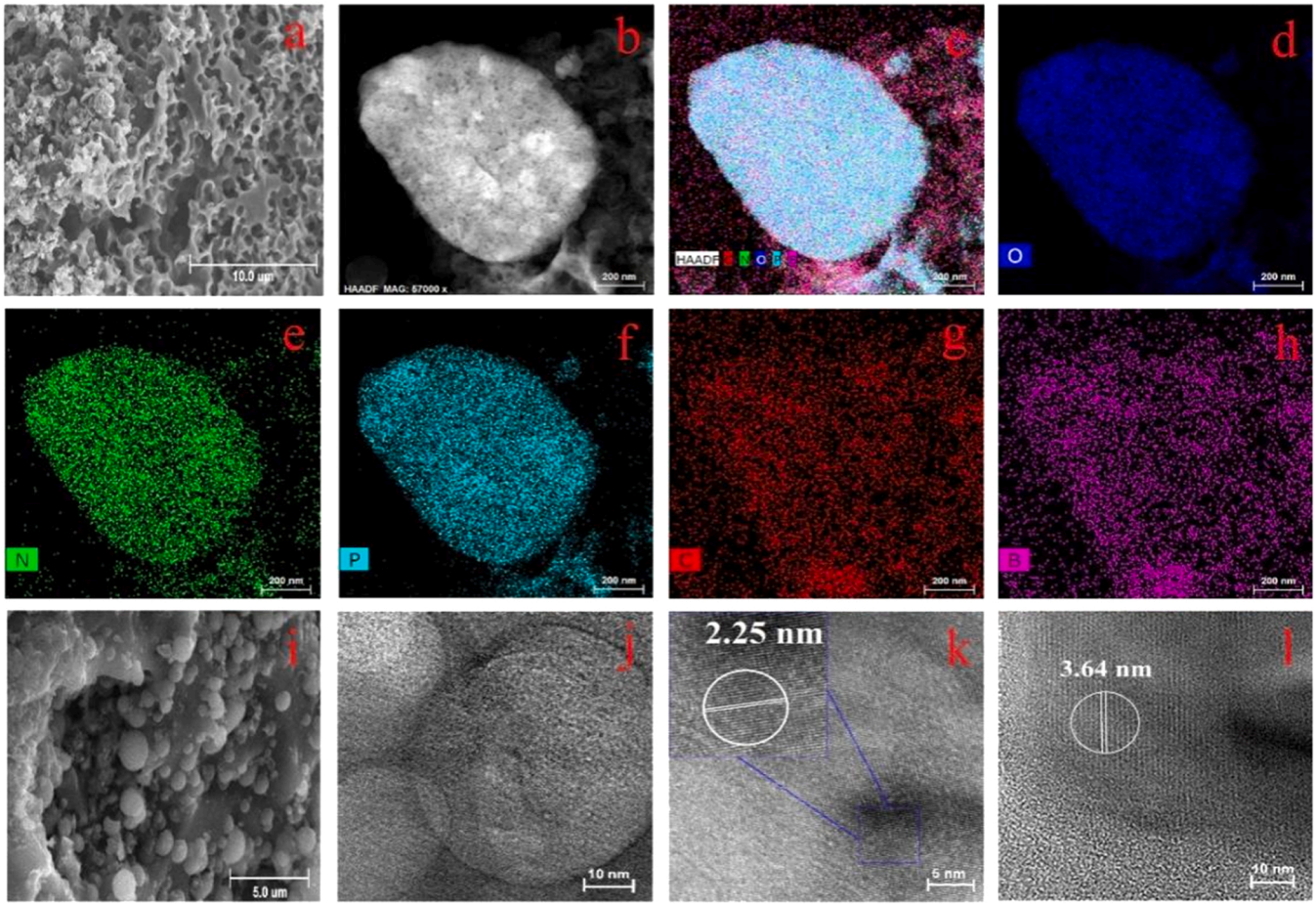

Fig. 3. (a) SEM image, (b) HAADF-STEM image and (c-h) STEM-EDS elemental mapping of BNP@C-800, (i) SEM image and (j-l) TEM images of BPO_4 in the BNP@C-800.

comparable with the reported metallic compounds at all. BNP@C-800 exhibited the highest catalytic activity with a 93.6% conversion of glycerol and 93.7% GC selectivity after 4 h. Without catalyst, the conversion of glycerol was only 33%. To our knowledge, this is the first report that the carbonylation of glycerol with urea could be effectively achieved over metal free catalyst. The catalytic performance (both conversion of glycerol and GC selectivity) of BNP@C-800 is even higher than that of the reported metallic catalysts operated under similar reaction conditions (in Fig. 6e). These results illustrate that the presence of active Lewis acid-base sites in the backbone of porous carbon could significantly improve its catalytic performance for GC production. Combined with HTEM, Raman and XPS spectra, a large number of defects on the surface of carbon materials lead to the formation of unsaturated coordination of B, N and P, which is favourable for the formation of Lewis acid-base sites. The presence of active Lewis acid-base sites on the catalyst surface may be the key factor to achieve higher activity than traditional metal-free carbon materials.

Owing to the high activities of BNP@C, we selected them as the model catalysts to probe the effects of carbonization temperatures and reaction temperature on the formation of GC. Firstly, we explored the catalytic performance of BNP@C-*T* ($T = 700$, 800, 900) catalysts with different carbonization temperatures. As shown in Fig. 6b and Table S2, three catalysts are able to achieve similar glycerol conversions within same reaction periods, but the GC selectivity over BNP@C-800 is higher than BNP@C-700 and BNP@C-900. Relatively few defect sites ($I_D/I_G = 1.14$) on the BNP@C-700, and sharp decreasing of active species (B, N and P) on BNP@C-900 were found from elemental content by Raman spectra and XPS characterization. While both factors will directly lead to the loss of Lewis acid-base sites, resulting in lower GC selectivity. Subsequently, the conversion and selectivity data of this catalytic reaction at the temperature ranging from 120 °C to 150 °C are shown in Fig. 6c and Table S3, which demonstrates that the glycerol conversion increases from 60.2% to 95.4% with the increase of reaction temperature. However, the GC selectivity increased from 72.9% at 120 °C to 93.7% at 140 °C and decreased to 75.21% at 150 °C. Under higher reaction temperature (150 °C), the generated GC could further react with urea to form II, resulting in a significant decrease in the GC selectivity.

Furthermore, BNP@C-800 catalyst could be easily recycled for five times only by simple washing and drying without obvious loss in catalytic activity (in Fig. 6d), confirming its good recyclability. The recycled BNP@C-800 catalyst was also characterized by FT-IR, XRD and XPS (in Figs. S7-S9), its crystalline phase and surface functional groups are nearly unchanged after recycle reaction test, which indicates the outstanding structural stability of BNP@C-800. Furthermore, the synthetic method of BNP@C-800 reproducible. We synthesized three batches of the BNP@ −800 materials and found that the basic characterization results (Figs. S10–12 and Table S4) and catalytic properties (Table S5) of other two batches were basically consistent with the first batch of BNP@C-800. Based on above results, BNP@C-800 catalyst exhibits remarkably high activity and selectivity in terms of glycerol conversion and GC selectivity. Moreover, BNP@C-800 is a robust, recyclable and reproducible metal-free catalyst for GC production, which is highly desirable for applied catalysis.

The React-IR was used to monitor the changes of functional groups in the carbonylation of glycerol with urea. Fig. 7a and b show the reaction spectra catalyzed by BNP@C-800 and BNP@C-900 as a function of

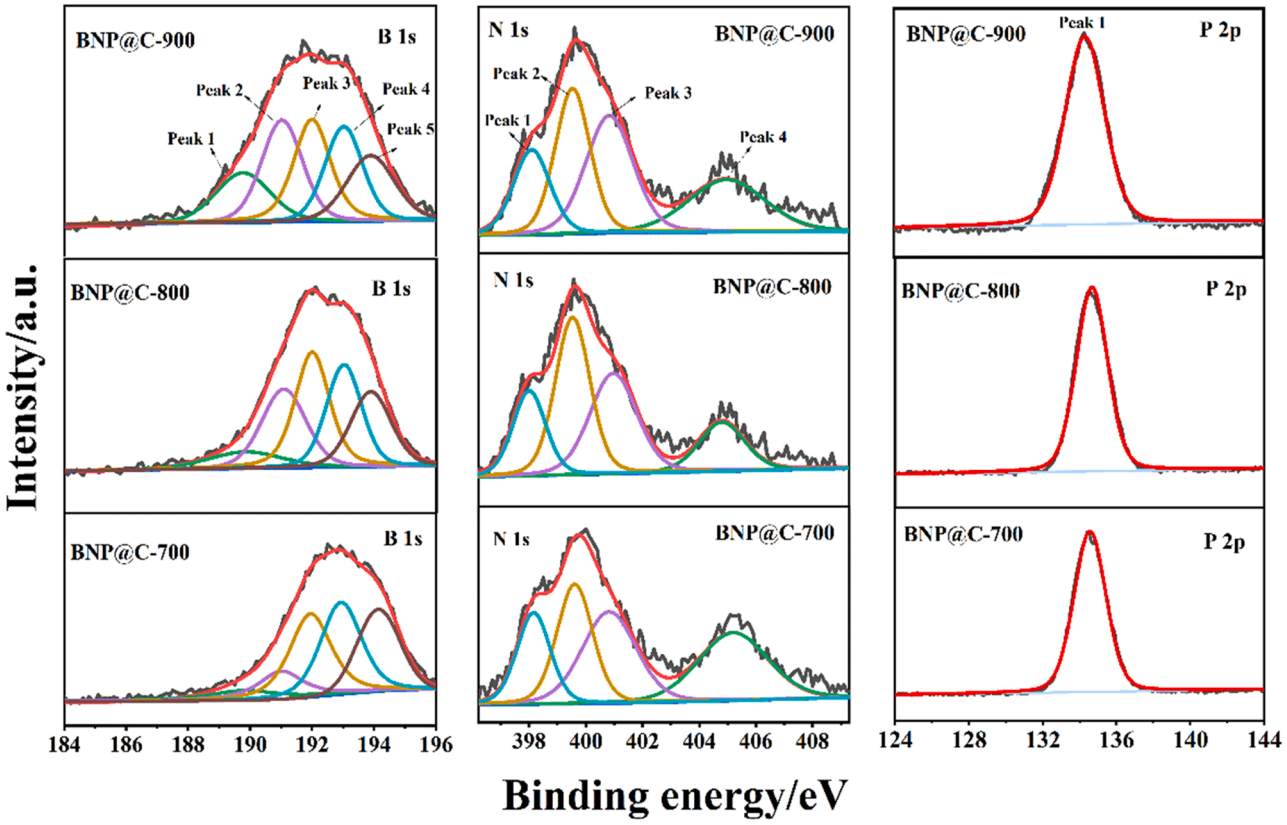

Fig. 4. XPS spectra: fine curves of B1s, N1s and P2p for BNP@C-*T* catalysts.

Table 2
The textural parameters of BNP@C-*T* materials.

Sample	Relative surface concentrations (at%)[a]					Acid group concentration (mmol/g)[b]	Basic group concentration (mmol/g)[b]
	C 1 s	N 1 s	O 1 s	P 2p	B 1 s		
BNP@C-700	35.68	3.87	30.35	6.50	23.60	0.36	0.11
BNP@C-800	37.45	3.49	29.71	6.36	22.99	0.37	0.10
BNP@C-900	52.48	4.45	22.88	4.21	15.98	0.31	0.16

[a] Determined by XPS spectra.
[b] Acidic and basic group concentrations obtained by titration.

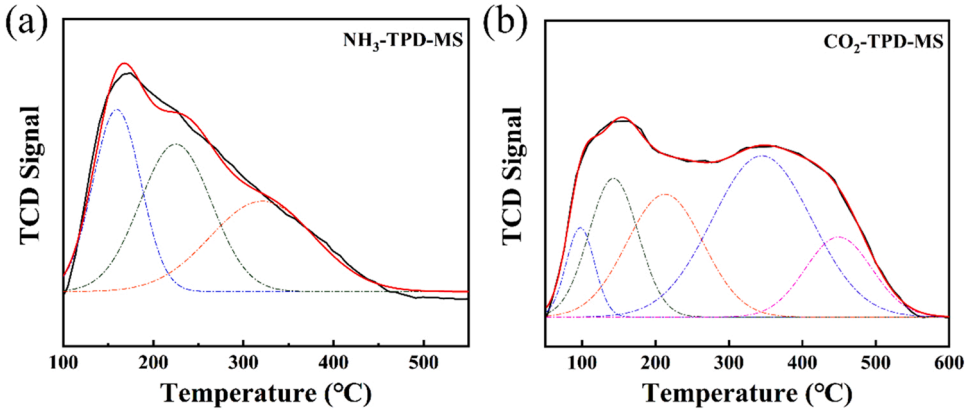

Fig. 5. NH_3- (a) and CO_2- (b) TPD-MS curves of BNP@C-800.

reaction time, respectively. The C═O stretching vibration, the N-H bending vibration and C-N stretching vibration of urea appear at the bands of 1664, 1610 and1440 cm^{-1}, respectively [56,57]. The C═O bond stretching vibration of GC product appears at 1784 cm^{-1} [58]. The peaks at 1404 and 1334 cm^{-1} could be attributed to the C-N and C-O stretching vibration of glycerol urethane by- intermediate product [59, 60]. With the change of reaction time, the intensities of 1663 and 1616 cm^{-1} in urea gradually decreased, while the intensity of the

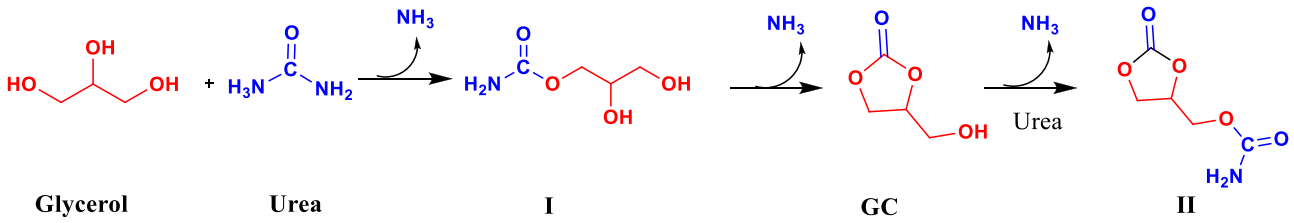

Scheme 2. Plausible reaction products for reaction between glycerol and urea, various products such as glycerol urethane (I), glycerol carbonate (GC), and (2-oxo-1,3-dioxolan-4-yl)methyl carbamate (II).

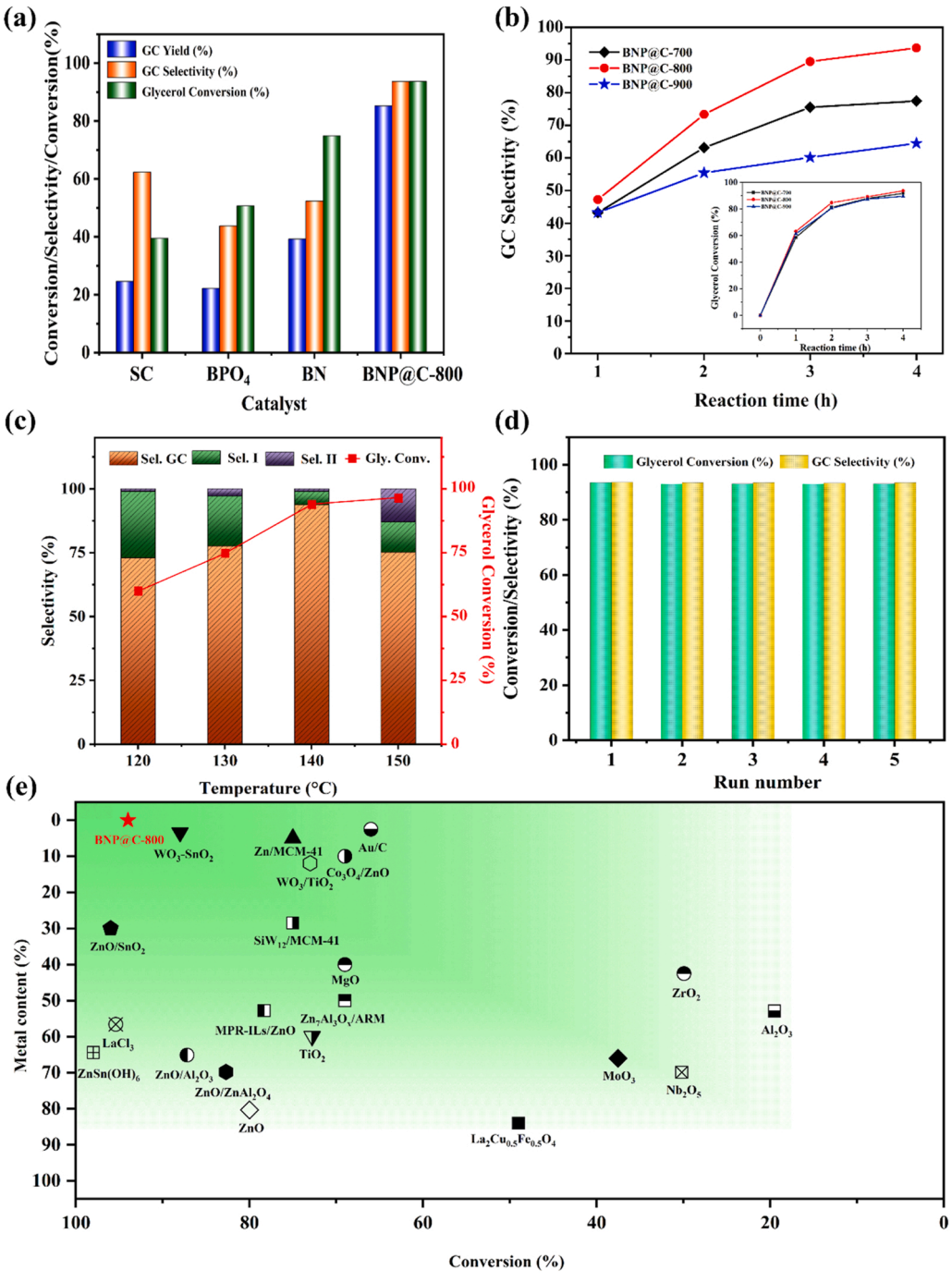

Fig. 6. Catalytic performance. (a) The catalytic performance comparison of different catalysts after 4 h reaction at 140 °C, (b) The effect of carbonization temperature on the catalytic performance at 140 °C, (c) The effect of reaction temperatures on the catalytic performance of BNP@C-800 at 140 °C for 4 h, (d) Recyclability and (e) Contrast diagram of catalytic performance. (Conditions: Reaction pressure = 7.0 kPa, glycerol/urea Ratio = 1:1.5).

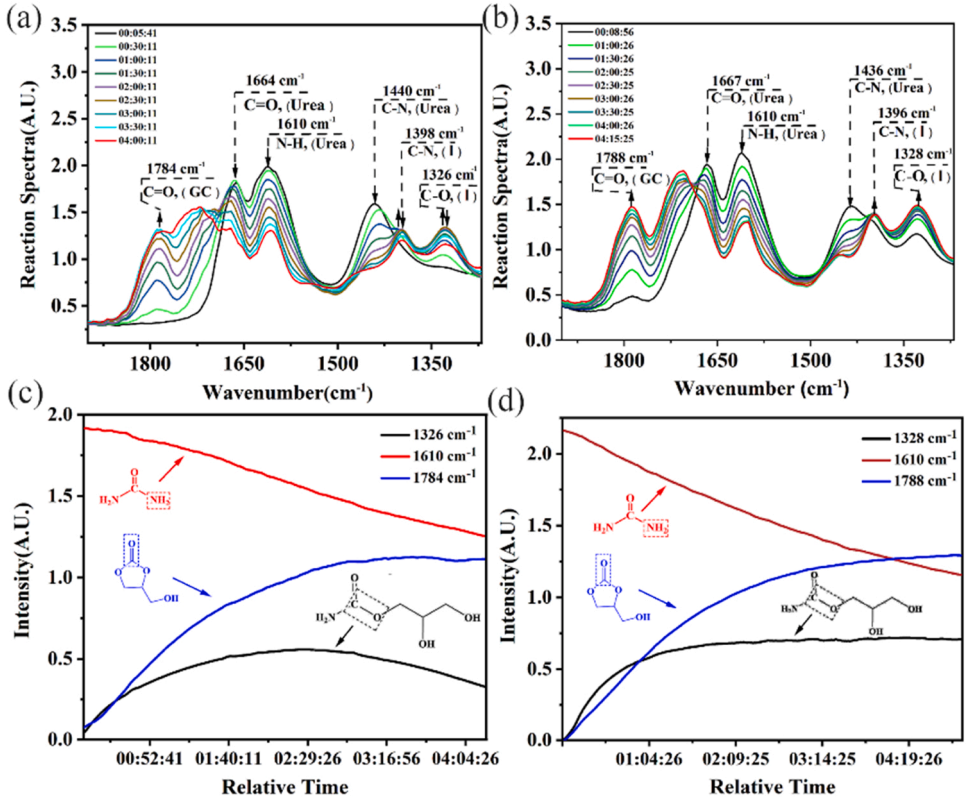

Fig. 7. Monitoring conversion of glycerol and urea to GC by in situ React IR. Conditions: reaction temperature = 140 °C, reaction pressure = 7.0 kPa, glycerol/urea Ratio = 1:1.5, catalyst: BNP@C-800 (a, c) and BNP@C-900 (b, d).

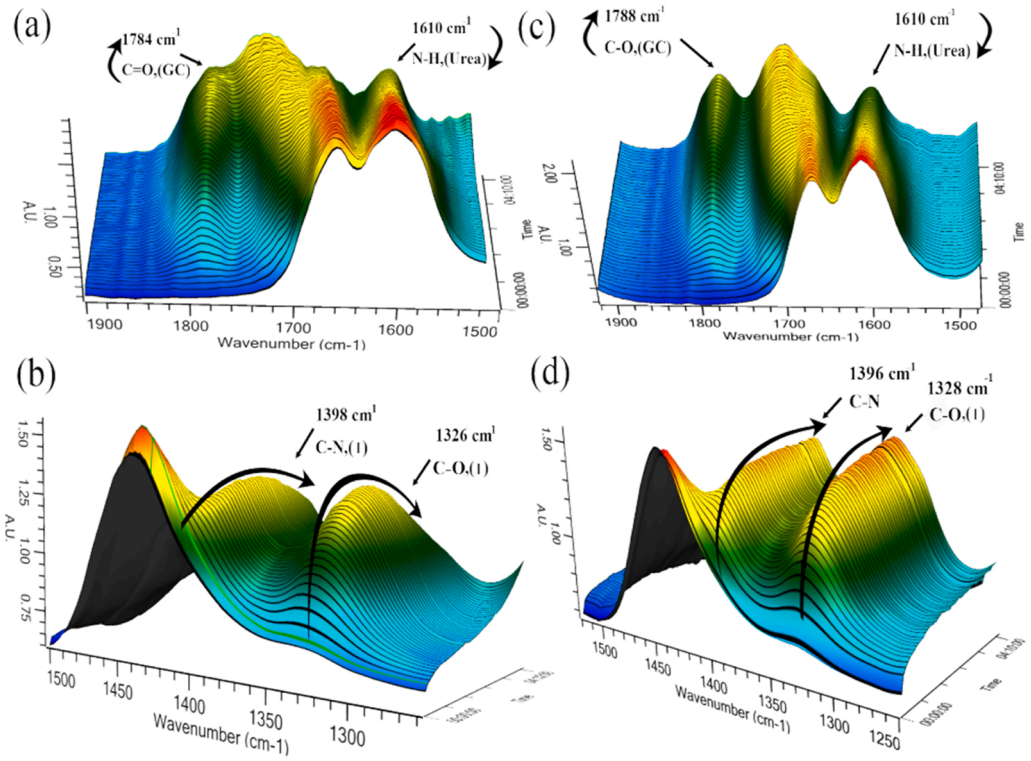

Fig. 8. . 3D-FTIR spectra. Conditions: reaction temperature = 140 °C, reaction pressure = 7.0 kPa, glycerol/urea Ratio = 1:1.5, catalyst: BNP@C-800 (a, b) and BNP@C-900 (c, d).

characteristic peak 1787 cm^{-1} of GC increased gradually, which indicates that urea reacted with glycerol to form the target product GC gradually. The change trend of representative absorptions corresponding to the characteristic groups of urea, glycerol urethane and GC in the reactions catalyzed by BNP@C-800 and BNP@C-900 are shown in Fig. 7c and d, respectively. As can be seen here, in both cases, two new absorption peaks at 1784 cm^{-1} and 1326 cm^{-1} were monitored in the reaction spectra, which correspond to C═O bond stretching vibration of GC and C-O stretching vibration of glycerol urethane intermediates, respectively. It is noteworthy that the amount of glycerol urethane intermediate in the reaction mixture catalyzed by BNP@C-800 (Fig. 6c) showed a trend of first increasing and then decreasing with the change of reaction time, which indicates that glycerol urethane was rapidly formed and then converted to GC. In contrast, the amount of glycerol urethane intermediate increases rapidly within 1 h and remains constant after 4 h over of BNP@C-900 catalyst (Fig. 7d), In addition, we find that when the GC yield increases slowly, the concentration of urea still decreases significantly, which is mainly used to react with GC to generate by-product II. In this process, urea occupies a part of limited active site, which inhibits the conversion of intermediate to target products, and finally leads to the decrease of selectivity of main products. Moreover, three-dimensional Fourier transform IR (3D-FTIR) spectra of the progressive carbonylation of glycerol with urea are presented in Fig. 8, which are more persuasive in combination with their corresponding 2D spectra. Combining Raman spectroscopy and XPS characterization, we found that similar defect levels were observed on BNP@C-800 and BNP@C-900, but with the increase of carbonization temperature, the content of B species with Lewis acid decreased significantly, which could be the main reason for the difference in catalytic activity between BNP@C-800 and BNP@C-900.

The catalysis reaction mechanism is not very clear. Usually, the catalytic performance of the catalysts originates from their unique structural feature. As mentioned before the structural defects have provided various LA/LB sites in the skeleton of BNP@C-*T* catalysts, which is confirmed by various techniques. Therefore, we propose a heterogeneous Lewis acid-base synergistic catalysis mechanism for glycerol carbonylation with urea as shown in Scheme 3. In the present case, it is reasonable to infer that a possible Lewis acid-base synergistic catalysis process between LA and LB active sites. The LB sites could deprotonate the hydroxyl group in glycerol to generate RO^- nucleophile, which could attack the carbonyl group of urea activated by LA sites in the skeleton of the catalyst. The H^+ dissociated from glycerol could be trapped by the amino groups of urea to give $-NH_3^+$ as a good leaving group. Release of NH_3 gas favors the first esterification reaction giving glycerol urethane intermediates with the regeneration of Lewis acidic/basic centers, which could continue to active the C═O and -OH groups in glycerol urethane to finally realize the intramolecular esterification reaction giving the cyclic GC product. Moreover, the unique porous character of BNP@C-800 catalyst must facilitate the release of GC product and NH_3 gas by-product, which kinetically favour the reaction conversion. Its appropriate spatial confinement effect would significantly stabilize the active Lewis acidic/basic sites on the skeleton of the material, meanwhile maintain excellent selectivity of GC product.

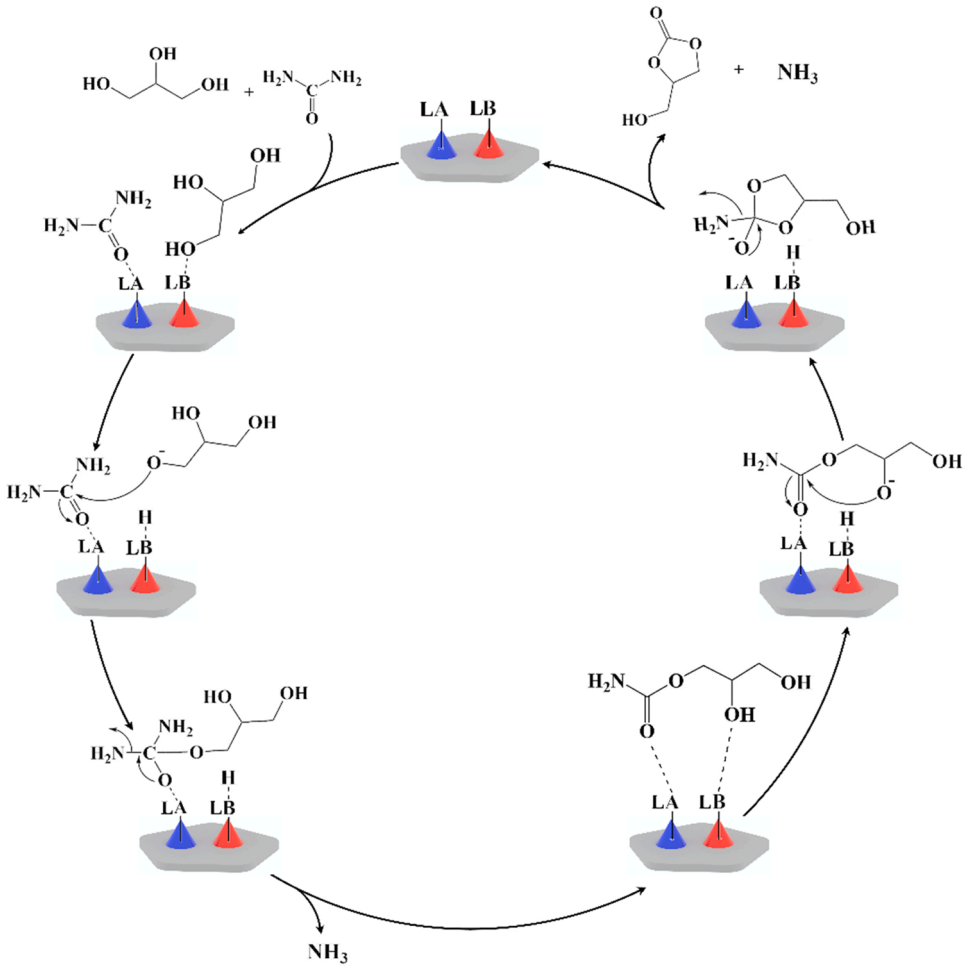

Scheme 3. Possible mechanism of the glycerol carbonylation with urea on the BNP@C-800 catalyst.

4. Conclusions

In summary, B,N,P co-doped porous carbon materials BNP@C were prepared by sol-gel method. The composition-optimized BNP@C-800 exhibited the highest catalytic activity with a 93.6% conversion of glycerol and 93.7% GC selectivity after 4 h at 140 °C and 7.0 kPa. It is because the structural defects provide various Lewis acid-base sites in the BNP@C-*T* catalyst skeleton that achieved efficient glycerol conversion and GC selectivity. This work highlights the catalytic role of active Lewis acid-base sites and provides guidance for GC production under practical industrial conditions. The introduction of active Lewis acid-base sites solves the problems in the conventional catalytic GC production, such as low activity, complex preparation, high cost, which conforms to the concept of green chemistry. Furthermore, this work also promotes the development of Lewis acid-base chemistry and porous carbon materials for applied catalysis.

CRediT authorship contribution statement

He Wang: Conceptualization, Methodology, Investigation, Formal analysis, Validation, Data curation, Writing – original draft. **Yunzuo Cui:** Conceptualization, Methodology, Investigation, Validation, Data curation. **Jinghui Shi**: Conceptualization, Writing – review & editing. **Xin Tao**: Conceptualization, Methodology, Resources, Writing – review & editing, Supervision, Funding acquisition. **Guangshan Zhu**: Conceptualization, Writing – review & editing.

Declaration of Competing Interest

The authors declare that they have no known competing financial interests or personal relationships that could have appeared to influence the work reported in this paper.

Data Availability

Data will be made available on request.

Acknowledgements

Financial supports from the National Natural Science Foundation of China (Grant No. 52173195, 22131004, U21A20330), the "111" project (B18012), Jilin Provincial Department of Science and Technology (20210508048RQ) and the Fundamental Research Funds for the Central Universities are gratefully acknowledged.

Appendix A. Supporting information

Supplementary data associated with this article can be found in the online version at doi:10.1016/j.apcatb.2023.122457.

References

[1] X.L. Luo, X.M. Ge, S.Q. Cui, Y.B. Li, Value-added processing of crude glycerol into chemicals and polymers, Bioresour. Technol. 215 (2016) 144–154, https://doi.org/10.1016/j.biortech.2016.03.042.
[2] A. Abbaszaadeh, B. Ghobadian, M.R. Omidkhah, G. Najafi, Current biodiesel production technologies: a comparative review, Energy Convers. Manag. 63 (2012) 138–148, https://doi.org/10.1016/j.enconman.2012.02.027.
[3] G.L. Brett, Q. He, C. Hammond, P.J. Miedziak, N. Dimitratos, M. Sankar, A. A. Herzing, M. Conte, J.A. Lopez-Sanchez, C.J. Kiely, D.W. Knight, S.H. Taylor, G. J. Hutchings, Selective oxidation of glycerol by highly active bimetallic catalysts at ambient temperature under base-Free conditions, Angew. Chem. Int. Ed. 50 (2011) 10136–10139, https://doi.org/10.1002/ange.201101772.
[4] M. Pagliaro, R. Ciriminna, H. Kimura, M.R. Prof, C.D. Pina, From glycerol to value-added products, Angew. Chem. Int. Ed. 46 (2007) 4434–4440, https://doi.org/10.1002/anie.200604694.
[5] Y. Nakagawa, Y. Shinmi, S. Koso, K. Tomishige, Direct hydrogenolysis of glycerol into 1,3-propanediol over rhenium-modified iridium catalyst, J. Catal. 272 (2010) 191–194, https://doi.org/10.1016/j.jcat.2010.04.009.
[6] C.H.C. Zhou, J.N. Beltramini, Y.X. Fan, G.Q.M. Lu, Chemoselective catalytic conversion of glycerol as a biorenewable source to valuable commodity chemicals, Chem. Soc. Rev. 37 (2008) 527–549, https://doi.org/10.1039/B707343G.
[7] Q. Li, W. Zhang, N. Zhao, W. Wei, Y. Sun, Synthesis of cyclic carbonates from urea and diols over metal oxides, Catal. Today 115 (2006) 111–116, https://doi.org/10.1016/j.cattod.2006.02.033.
[8] J.R. Ochoa-Gómez, O. Gómez-Jiménez-Aberasturi, C. Ramírez-López, M. Belsué, A brief review on industrial alternatives for the manufacturing of glycerol carbonate, a green chemical, Org. Process Res. Dev. 16 (2012) 389–399, https://doi.org/10.1021/op200369v.
[9] A. Dibenedetto, A. Angelini, M. Aresta, J. Ethiraj, C. Fragale, F. Nocito, Converting wastes into added value products: from glycerol to glycerol carbonate, glycidol and epichlorohydrin using environmentally friendly synthetic routes, Tetrahedron 67 (2011) 1308–1313, https://doi.org/10.1016/j.tet.2010.11.070.
[10] A. Wang, H. Li, H. Pan, H. Zhang, F.S. Xu, Z.Z. Yu, S. Yang, Efficient and green production of biodiesel catalyzed by recyclable biomass-derived magnetic acids, Fuel Process. Technol. 181 (2018) 259–267, https://doi.org/10.1016/j.fuproc.2018.10.003.
[11] A. Devarajan, S. Thiripuranthagan, R. Radhakrishnan, S. Kumaravel, Solvent free transesterification of glycerol into glycerol carbonate over nanostructured CaAl hydrotalcite catalyst, J. Nanosci. Nanotechnol. 18 (2018) 4588–4599, https://doi.org/10.1166/jnn.2018.15265.
[12] H.G. Li, D.Z. Gao, P. Gao, F. Wang, N. Zhao, F.K. Xiao, W. Wei, Y.H. Sun, The synthesis of glycerol carbonate from glycerol and CO_2 over $La_2O_2CO_3$-ZnO catalysts, Catal. Sci. Technol. 3 (2013) 2801–2809, https://doi.org/10.1039/C3CY00335C.
[13] C.Y. Park, H. Nguyen-Phu, E.W. Shin, Glycerol carbonation with CO_2 and $La_2O_2CO_3$/ZnO catalysts prepared by two different methods: preferred reaction route depending on crystalline structure, Mol. Catal. 435 (2017) 99–109, https://doi.org/10.1016/j.mcat.2017.03.025.
[14] P. Manjunathan, R. Ravishankar, G.V. Shanbhag, Novel bifunctional Zn-Sn composite oxide catalyst for the selective synthesis of glycerol carbonate by carbonylation of glycerol with urea, ChemCatChem 8 (2016) 631–639, https://doi.org/10.1002/cctc.201501088.
[15] M. Aresta, A. Dibenedetto, F. Nocito, C. Ferragina, Valorization of bio-glycerol: new catalytic materials for the synthesis of glycerol carbonate via glycerolysis of urea, J. Catal. 268 (2009) 106–114, https://doi.org/10.1016/j.jcat.2009.09.008.
[16] T.W. Turney, A. Patti, W. Gates, U. Shaheen, S. Kulasegaram, Formation of glycerol carbonate from glycerol and urea catalysed by metal monoglycerolates, Green. Chem. 15 (7) (2013) 1925–1931, https://doi.org/10.1039/C3GC37028C.
[17] G.P. Fernandes, G.D. Yadav, Selective glycerolysis of urea to glycerol carbonate using combustion synthesized magnesium oxide, Catal. Today 309 (2018) 153–160, https://doi.org/10.1016/j.cattod.2017.08.021.
[18] J.H. Park, J.S. Choi, S.K. Woo, S.D. Lee, M. Cheong, H.S. Kim, H. Lee, Isolation and characterization of intermediate catalytic species in the Zn-catalyzed glycerolysis of urea, Appl. Catal. A 433 (2012) 35–40, https://doi.org/10.1016/j.apcata.2012.04.031.
[19] Y.F. Sun, X.L. Tong, Z.D. Wu, J.B. Liu, Y.T. Yan, S. Xue, A sustainable preparation of glycerol carbonate from glycerol and urea catalyzed by hydrotalcite-like solid catalysts, Energy Technol. 2 (2014) 263–268, https://doi.org/10.1002/ente.201300135.
[20] V.S. Marakatti, A.B. Halgeri, Metal ion-exchanged zeolites as highly active solid acid catalysts for the green synthesis of glycerol carbonate from glycerol, RSC Adv. 5 (2015) 14286–14293, https://doi.org/10.1039/C4RA16052E.
[21] V.P. Indran, N.A.S. Zuhaimi, M.A. Deraman, G.P. Maniam, M.M. Yusoff, T.Y.Y. Hin, M.H.A. Rahim, An accelerated route of glycerol carbonate formation from glycerol using waste boiler ash as catalyst, RSC Adv. 4 (2014) 25257–25267, https://doi.org/10.1039/C4RA02910K.
[22] K. Jagadeeswaraiah, R. Kumar, A. Rajashekar, A. Srivani, N. Lingaiah, The role of tungsten oxide species supported on titania catalysts for the synthesis of glycerol carbonate from glycerol and urea, Catal. Lett. 146 (2016) 692–700, https://doi.org/10.1007/s10562-016-1694-9.
[23] D.W. Kim, M.J. Kim, K. Roshith, M.I. Kim, J.Y. Kwak, D.W. Park, Comparative catalytic activity of supported $ZnBr_2$-containing ionic liquid catalysts for preparation of glycerol carbonate by glycerolysis of urea, Korean J. Chem. Eng. 31 (2014) 972–980, https://doi.org/10.1007/s11814-013-0296-0.
[24] S.E. Kondawar, A.S. Potdar, C.V. Rode, Solvent-free carbonylation of glycerol with urea using metal loaded MCM-41 catalysts, RSC Adv. 5 (2015) 16452–16460, https://doi.org/10.1039/C4RA11590B.
[25] S.D. Lee, G.A. Park, D.W. Kim, D.W. Park, Catalytic performance of functionalized IRMOF-3 for the synthesis of glycerol carbonate from glycerol and urea, J. Nanosci. Nanotechnol. 14 (2014) 4551–4556, https://doi.org/10.1166/jnn.2014.8255.
[26] D.W. Kim, K.A. Park, M.J. Kim, D.H. Kang, J.G. Yang, D.W. Park, Synthesis of glycerol carbonate from urea and glycerol using polymer-supported metal containing ionic liquid catalysts, Appl. Catal. A 473 (2014) 31–40, https://doi.org/10.1016/j.apcata.2013.12.032.
[27] M. Aresta, A. Dibenedetto, F. Nocito, C. Ferragina, Valorization of bio-glycerol: New catalytic materials for the synthesis of glycerol carbonate via glycerolysis of urea, J. Catal. 268 (2009) 106–114, https://doi.org/10.1016/j.jcat.2009.09.008.
[28] L.G. Wang, Y.B. Ma, Y. Wang, S.M. Liu, Y.Q. Deng, Efficient synthesis of glycerol carbonate from glycerol and urea with lanthanum oxide as a solid base catalyst, Catal. Commun. 12 (2011) 1458–1462, https://doi.org/10.1016/j.catcom.2011.05.027.
[29] J. Zhang, D.H. He, Lanthanum-based mixed oxides for the synthesis of glycerol carbonate from glycerol and urea, React. Kinet. Catal. Lett. 113 (2014) 375–392, https://doi.org/10.1007/s11144-014-0739-6.

[30] H.Y. Ji, D.P. Song, B. Wang, L. Pan, Y.S. Li, Organic Lewis pairs for selective copolymerization of epoxides with anhydrides to access sequence-controlled block copolymers, Green. Chem. 21 (22) (2019) 6123–6132, https://doi.org/10.1039/C9GC02429H.
[31] Q. Zhang, Y. Li, L. Zhang, S. Luo, Catalytic asymmetric disulfuration by a chiral bulky three-component Lewis acid-base, Angew. Chem. Int. Ed. 133 (19) (2021) 11066–11071, https://doi.org/10.1002/ange.202101569.
[32] X.R. Tian, X.L. Jiang, S.L. Hou, Z.H. Jiao, J. Han, B. Zhao, Selectively regulating Lewis acid-base sites in metal-organic frameworks for achieving turn-on/off of the catalytic activity in different CO_2 reactions, Angew. Chem. Int. Ed. 134 (18) (2022), e202200123, https://doi.org/10.1002/ange.202200123.
[33] H. Zhang, H. Zhao, S. Zhai, R. Zhao, J. Wang, X. Cheng, H.S. Shiran, S.R. Larter, M. G. Kibria, J. Hu, Electron-enriched Lewis acid-base sites on red carbon nitride for simultaneous hydrogen production and glucose isomerization, Appl. Catal. B: Environ. 316 (2022), 121647, https://doi.org/10.1016/j.apcatb.2022.121647.
[34] Y. Ding, X. Huang, X. Yi, Y. Qiao, X. Sun, A. Zheng, D.S. Su, A Heterogeneous Metal-Free catalyst for hydrogenation: Lewis acid-base pairs integrated into a carbon lattice, Angew. Chem. Int. Ed. 57 (42) (2018) 13800–13804, https://doi.org/10.1002/anie.201803977.
[35] W. Song, Y. Zhang, A. Varyambath, I. Kim, Guided assembly of well-defined hierarchical nanoporous polymers by lewis acid-base interactions, ACS Nano 13 (10) (2019) 11753–11769, https://doi.org/10.1021/acsnano.9b05727.
[36] Y.R. Wang, J. Sheng, W.D. Lu, B. Yan, A.H. Lu, A highly selective metal-free boron-based catalyst for oxidative dehydrogenation of ethylbenzene, Chin. J. Chem. 39 (2021) 2563–2569, https://doi.org/10.1002/cjoc.202100283.
[37] B.J. Xu, J. Long, H.P. Tian, Y.X. Zhu, X. Sun, Synthesis and characterization of mesoporous γ-alumina templated by saccharide molecules, Catal. Today 147 (2009) S46–S50, https://doi.org/10.1016/j.cattod.2009.07.059.
[38] A. Saha, A. Mondal, S. Maiti, S.C. Ghosh, S. Mahanty, A.B. Panda, A facile method for the synthesis of a C@ MoO_2 hollow yolk-shell structure and its electrochemical properties as a faradaic electrode, Mater. Chem. Front. 1 (2017) 1585–1593, https://doi.org/10.1039/C7QM00006E.
[39] R. Atchudan, T.N.J.I. Edison, S. Perumal, Y.R. Lee, Green synthesis of nitrogen-doped graphitic carbon sheets with use of Prunus persica for supercapacitor applications, Appl. Surf. Sci. 393 (2017) 276–286, https://doi.org/10.1016/j.apsusc.2016.10.030.
[40] E. Çakmakçı, A. Güngör, Preparation and characterization of flame retardant and proton conducting boron phosphate/polyimide composites, Polym. Degrad. Stab. 98 (2013) 927–933, https://doi.org/10.1016/j.polymdegradstab.2013.03.003.
[41] Z.M. Xue, X.H. Zhao, J.F. Wang, T.C. Mu, Bifunctional boron phosphate as an efficient catalyst for epoxide activation to synthesize cyclic carbonates with CO_2, Chem. Asian J. 12 (2017) 2271–2277, https://doi.org/10.1002/asia.201700688.
[42] R. Wang, H. Jiang, H. Gong, J. Zhang, Synthesis of nanosize BPO_4 under microwave irradiation, Mater. Res. Bull. 47 (2012) 2108–2111, https://doi.org/10.1016/j.materresbull.2012.04.028.
[43] X.L. Yuan, M. Zhang, X.D. Chen, N.H. An, G. Liu, Y. Liu, W.X. Zhang, W.F. Yan, M. J. Jia, Transesterification of dimethyl oxalate with phenol over nitrogen-doped nanoporous carbon materials, Appl. Catal. A Gen. 439–440 (2012) 149–155, https://doi.org/10.1016/j.apcata.2012.06.052.
[44] S.L. Wang, M. Xu, T.Y. Peng, C.X. Zhang, T. Li, I. Hussain, J.Y. Wang, B. Tan, Porous hypercrosslinked polymer-TiO_2-graphene composite photocatalysts for visible-light-driven CO_2 conversion, Nat. Commun. 10 (2019) 1–10, https://doi.org/10.1038/s41467-019-08651-x.
[45] J. Jiang, L. Zhang, X. Wang, N. Holm, K. Rajagopalan, F. Chen, S. Ma, Highly ordered macroporous woody biochar with ultra-high carbon content as supercapacitor electrodes, Electrochim. Acta 113 (2013) 481–489, https://doi.org/10.1016/j.electacta.2013.09.121.
[46] C. Kalinke, P.R. Oliveira, G.A. Oliveira, A.S. Mangrich, L.H. Marcolino-Junior, M. F. Bergamini, Activated biochar: preparation, characterization and electroanalytical application in an alternative strategy of nickel determination, Anal. Chim. Acta 983 (2017) 103–111, https://doi.org/10.1016/j.aca.2017.06.025.
[47] C. Van Nguyen, S. Lee, Y.G. Chung, W.H. Chiang, K.C.W. Wu, Synergistic effect of metal-organic framework-derived boron and nitrogen heteroatom-doped three-dimensional porous carbons for precious-metal-free catalytic reduction of nitroarenes, Appl. Catal. B: Environ. 257 (2019), 117888, https://doi.org/10.1016/j.apcatb.2019.117888.
[48] G. Liu, Y. Liu, X.Y. Zhang, X.L. Yuan, M. Zhang, W.X. Zhang, M.J. Jia, Characterization and catalytic performance of porous carbon prepared using in situ-formed aluminophosphate framework as template, J. Colloid Interf. Sci. 342 (2010) 467–473, https://doi.org/10.1016/j.jcis.2009.10.036.
[49] R. Arrigo, M. Hävecker, S. Wrabetz, R. Blume, M. Lerch, J. McGregor, E.P. J. Parrott, J.A. Zeitler, L.F. Gladden, A.K. Gericke, R. Schlögl, D.S. Su, Tuning the acid/base properties of nanocarbons by functionalization via amination, J. Am. Chem. Soc. 132 (2010) 9616–9630, https://doi.org/10.1021/ja910169v.
[50] Y.N. Chang, H.F. Shi, X.L. Yan, G.X. Zhang, L. Chen, A ternary B, N, P-Doped carbon material with suppressed water splitting activity for high-energy aqueous supercapacitors, Carbon 170 (2020) 127–136, https://doi.org/10.1016/j.carbon.2020.08.013.
[51] W.D. Lu, X.Q. Gao, Q.G. Wang, W.C. Li, Z.C. Zhao, D.Q. Wang, A.H. Lu, Ordered macroporous boron phosphate crystals as metal-free catalysts for the oxidative dehydrogenation of propane, Chin. J. Catal. 41 (2020) 1837–1845, https://doi.org/10.1016/S1872-2067(20)63654-3.
[52] B.H. Cheng, L.J. Deng, J. Jiang, H. Jiang, Catalytic cycloaddition of CO_2 to epoxides by the synergistic effect of acidity and alkalinity in a functionalized biochar, Chem. Eng. J. 442 (2022), 136265, https://doi.org/10.1016/j.cej.2022.136265.
[53] Z. Yu, Y. Yang, S. Yang, J. Zheng, X. Hao, G. Wei, H. Bai, A. Abudula, G. Guan, Selective dehydrogenation of aqueous formic acid over multifunctional γ-Mo_2N catalysts at a temperature lower than 100 °C, Appl. Catal. B: Environ. 313 (2022), 121445, https://doi.org/10.1016/j.apcatb.2022.121445.
[54] M. Sevilla, P. Valle-Vigon, A.B. Fuertes, N-Doped polypyrrole-based porous carbons for CO_2 capture, Adv. Funct. Mater. 21 (2011) 2781–2787, https://doi.org/10.1016/j.jece.2021.106452.
[55] D. Liu, S. Kang, Y. Xu, P. Duan, S. Chen, Core-shell catalyst with synergistic hydroxyl and nitrogen active sites for CO_2 cycloaddition, J. Environ. Chem. Eng. 9 (6) (2021), 106452, https://doi.org/10.1016/j.jece.2021.106452.
[56] Q.B. Li, W.Y. Zhang, N. Zhao, W. Wei, Y.H. Sun, Synthesis of cyclic carbonates from urea and diols over metal oxides, Catal. Today 115 (2006) 111–116, https://doi.org/10.1016/j.cattod.2006.02.033.
[57] S.H. Overbury, A.I. Kolesnikov, G.M. Brown, Z.Y. Zhang, G.S. Nair, R.L. Sacci, R. Lotfi, A.C.T. van Duin, M. Naguib, Complexity of intercalation in MXenes: Destabilization of urea by two-dimensional titanium carbide, J. Am. Chem. Soc. 140 (2018) 10305–10314, https://doi.org/10.1021/jacs.8b05913.
[58] H. An, Y. Ma, X. Zhao, Y. Wang, Preparation of Zn–Al oxide catalyst and its catalytic performance in propylene carbonate synthesis from urea and propylene glycol on a fixed-bed reactor, Catal. Today 264 (2016) 136–143, https://doi.org/10.1016/j.cattod.2015.09.006.
[59] D. Shee, G. Deo, In situ DRIFT studies of alkane adsorption on vanadia supported titania-doped catalysts, Catal. Today 325 (2019) 25–32, https://doi.org/10.1016/j.cattod.2018.06.003.
[60] E.S. Dragan, M.V. Dinu, G. Lisa, A.W. Trochimczuk, Study on metal complexes of chelating resins bearing iminodiacetate groups, Eur. Polym. J. 45 (2009) 2119–2130, https://doi.org/10.1016/j.eurpolymj.2009.03.012.